Dynamic Analysis of Cascaded Laser Power Converters for Simultaneous High-Speed Data Detection and Optical-to-Electrical DC Power Generation

Jin-Wei Shi, F.-M. Kuo, Chan-Shan Yang, S.-S. Lo, and Ci-Ling Pan, *Senior Member, IEEE*

***Abstract*—We analyze the dynamic behaviors of a novel device, i.e., cascaded high-speed laser power converters (LPCs), which can detect the direct-current (dc) component of an incoming high-speed optical data stream and efficiently convert its dc component to dc electrical power. By utilizing a p-type photoabsorption layer in our LPC, the problem of slow-motion holes can be eliminated, and only the electrons act as the active carriers. We can thus achieve high-speed performance with the LPC under forward-bias operation with a small electric field inside. Furthermore, according to our modeling and measurement results, there are a significant alternating-current capacitance reduction and an electron-trapping effect at the interface between the absorption and collector layers with a significant degradation in the carrier drift velocity. These become more serious with the increase in optical pumping power and forward-bias voltage and truly limit the net optical-to-electrical (O–E) bandwidth of the device. In order to overcome such a transient-time-limited bandwidth and further increase the maximum dc output voltage of the LPC, we connect two single LPCs in series (cascade). Error-free data detection of 10-Gb/s and an O–E dc power-generation efficiency of 21.1% can be achieved simultaneously at a wavelength of 850 nm by the use of such two cascaded LPCs.**

***Index Terms*—Photodiodes (PDs), photovoltaic.**

I. Introduction

RECENTLY, the development of optical-interconnect (OI) techniques [1]–[4], which could allow the replacement of bulky and power-hungry active/passive microwave components with more energy-saving and high-speed optoelectronic devices, has become an attractive choice to realize the ideal of the "Green Internet" [5]. In exascale supercomputers, the OI technique plays a key role in meeting challenging technological and economic requirements. In future supercomputers, the estimated total power consumption and bandwidth for an OI system could be as high as 8 MW and 400 PB/s, respectively [6]. The reduction of the power required to feed the high-speed vertical-cavity surface-emitting laser (VCSEL) at the transmitting end is one effective way to further reduce the overall power consumption. On the other hand, the direct-current (dc) component of the high-speed optical data signal at the receiving end is usually wasted due to the fact that, in traditional p-i-n photodiodes (PDs), reverse-bias operation is necessary, which will result in the power consumption with excess heat generation during high-speed optical data detection. Recently, the unitraveling-carrier PD (UTC PD) structure has been used to achieve reasonable high-speed and high-responsivity performance under zero-bias operation [7]–[9]. Such devices have been demonstrated to eliminate the excess power consumption. In this paper, we analyze in detail the dynamic behaviors of a novel device, i.e., the linear cascaded GaAs/AlGaAs-based high-speed laser power converter (LPC) [10]–[13], by the use of the equivalent-circuit modeling technique [14]. Such a device exhibits the performance of a high-speed PD even when its operating voltage is further pushed to the forward bias. We can thus generate (instead of consuming) dc electrical power by using this device during high-speed data transmission in an OI system. By the use of the equivalent-circuit modeling technique, we found that the significant alternating-current (ac) capacitance reduction effect happens [14] and the slow internal carrier transient time is the dominant bandwidth-limiting factor of a single LPC under a forward-bias voltage of > 0.5 V. In order to further boost the operating speed and maximum output dc voltage of our device, we connect two single LPCs in series. According to the modeling result, our cascaded structure can effectively minimize the internal carrier drift time. This is due to the larger built-in field compared with that of a single LPC even when operated under the same output current and forward bias (i.e., $+1$ V). Error-free optical data detection of 10 Gb/s (or 5 Gb/s) with an optical-to-electrical (O–E) power-generation efficiency of 21.1% (or 34%) can be simultaneously achieved using our device with the cascaded structure at an optical wavelength of 850 nm.

Manuscript received January 21, 2011; revised March 21, 2011 and March 23, 2011; accepted March 25, 2011. Date of publication April 21, 2011; date of current version June 22, 2011. This work was supported in part by the National Science Council of Taiwan under Grant 99-2221-E-008-027-MY3 and Grant 98-2221-E-008-009-MY3 and in part by the Ministry of Economic Affairs of Taiwan under Grant 98-EC-17-A-07-S1-001. The review of this paper was arranged by Editor A. G. Aberle.

J.-W. Shi and F.-M. Kuo are with the Department of Electrical Engineering, National Central University, Taoyuan 320, Taiwan, and also with the Department of Electrical and Computer Engineering, University of California Santa Barbara, Santa Barbara, CA 93106 USA (e-mail: jwshi@ee.ncu.edu.tw; jwshi@ece.ucsb.edu).

C.-S. Yang and C.-L. Pan are with the Department of Physics, National Tsing Hua University, Hsinchu 300, Taiwan.

S.-S. Lo is with the Department of Photonics and Institute of Electro-Optics, National Chiao Tung University, Hsinchu 300, Taiwan.

Color versions of one or more of the figures in this paper are available online at http://ieeexplore.ieee.org.

Digital Object Identifier 10.1109/TED.2011.2136379

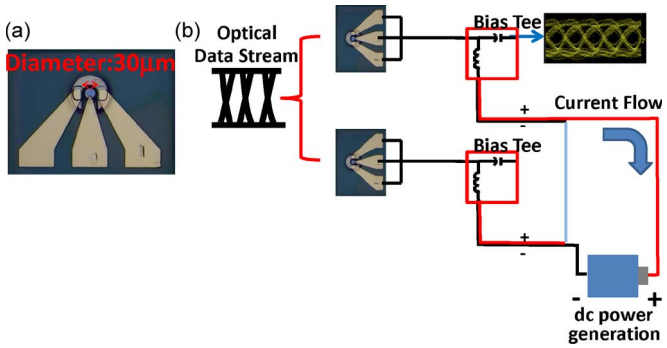

Fig. 1. (a) Top view of the single device. (b) Conceptual view of the linear cascaded device of the demonstrated high-speed LPC.

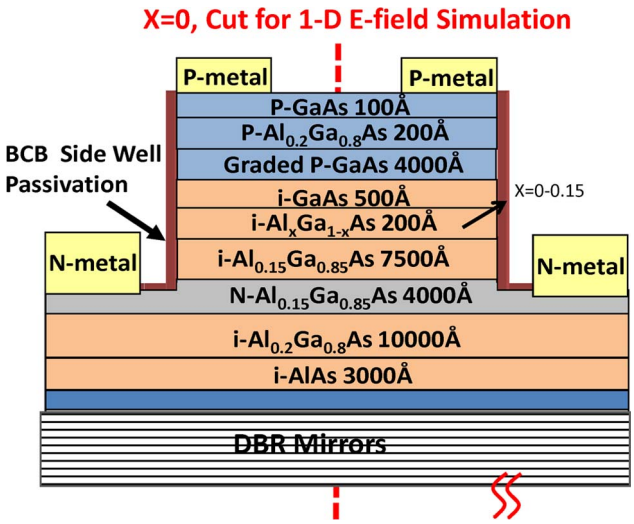

Fig. 2. Cross-sectional view of the demonstrated high-speed LPC.

II. Device Structure

Fig. 1(a) and (b) shows the top view of a single LPC and a conceptual diagram of the linear cascaded LPCs, respectively. Fig. 2 shows a cross-sectional view of the fabricated device. We adopted a typical vertical-illuminated PD structure with an active circular mesa and a p-type ring contact on the top. The diameter of the whole mesa and the inner circle for light illumination were 28 and 20 μm, respectively. As shown in Fig. 2, the epitaxial-layer (epi-layer) structure of our device is similar to that reported for our GaAs/AlGaAs-based UTC PD [8], [9] at the wavelength of 850 nm. The device mainly consists of a p-type GaAs-based photoabsorption layer with a thickness of 450 nm and an undoped $Al_{0.15}Ga_{0.85}As$-based collector layer with a thickness of 750 nm. A graded p-doped profile [from 1×10^{19} (top) to 1×10^{17} cm^{-3} (bottom)] is used in the absorption layer to accelerate the diffusion velocity of the photogenerated electrons. Compared with the traditionally structured p-i-n PD, we can expect much higher speed performance under zero- or forward-bias operation because there are only electrons in the active carrier. This means that the device can exhibit a much faster drift velocity than that of the hole in the p-i-n PD under a small electric field (e-field) (i.e., $\sim$10 kV/cm) [7]. As shown in Fig. 2, the whole epi-layer structure of the LPC was grown on an n-type distributed Bragg reflector to enhance its responsivity performance. The main drawback of the photovoltaic LPC is its low output voltage, which is usually too low to directly power other active components in the OI system. In order to boost the dc operating voltage of our LPC, several high-speed LPCs are series wound (linear cascade). The dc operation voltage would thus be proportional to the number of cascaded units [11]–[13]. In addition, in order to maximize the net output photocurrent, the output photocurrent from each cascaded unit must be as close as possible [11]–[13]. The series connection and current balancing of the different cascaded PD units leads to a reduction in the total capacitance, and a significant improvement in the O–E bandwidth has thus been demonstrated [15], [16]. However, in this case, the measured net O–E bandwidth is very sensitive to the amount of injected optical power onto different PDs [16]. Fig. 1(b) shows a conceptual diagram of the linear cascaded two-LPC device. As shown, in order to eliminate the serious influence of the optical power on the measured O–E bandwidth of the cascaded two-LPC device, we use two bias tees to let the two LPCs be series-wound only in their dc part. The output photogenerated radio-frequency (RF) signal is extracted from one of the two LPCs. We can thus expect that the dynamic performance of the cascaded device would be similar to that of the single device. The main difference would be that the dc turn-on voltage of the cascaded device would be twice higher than that of the single device.

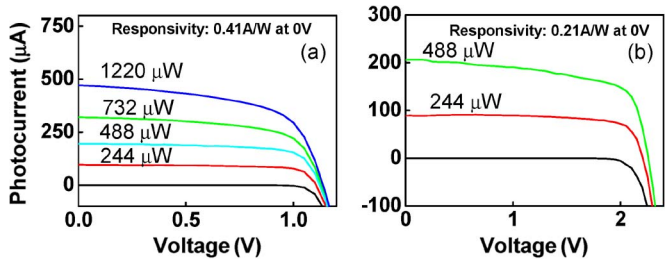

Fig. 3. (a) Measured I–V curves of the (a) single and (b) linear cascaded devices under different optical pumping power values.

III. Measurement Results and Discussion

The measured dc responsivity of our single device is around 0.41 A/W, which corresponds to around an external quantum efficiency of 60% under zero-bias operation. Under low-power injection (i.e., $<$ 0.5 mW), there is a slight degradation in this value to around 0.36 A/W when the operating voltage reaches $+0.9$ V. A lightwave-component-analyzer system was utilized to characterize the dynamic performance of the device under continuous-wave operation by measuring the frequency responses of the scattering (S) parameters. We employed a tunable semiconductor laser operated at 830 nm as the light source for this system. The optical signal was injected into the device by using a 2.5-μm spot diameter lens fiber. Fig. 3(a) and (b) shows the measured current–voltage (I–V) curves of the single-LPC and linear cascaded two-LPC devices under different output photocurrents. The value of the injected optical power to each single device is specified in traces (a) and (b). As shown, the operating voltage of the cascaded device is about

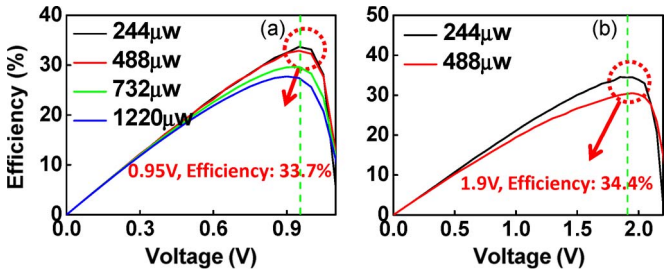

Fig. 4. Measured O–E power-conversion efficiency versus bias voltage of (a) the single and (b) linear cascaded devices under different optical pumping power values.

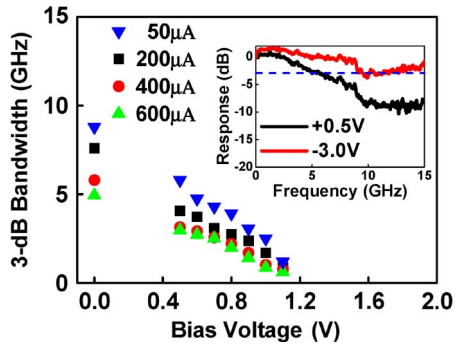

Fig. 5. Measured 3-dB O–E bandwidth versus forward-bias voltage for the single device under different output photocurrents. The inset shows the measured O–E frequency responses of the single device under forward- and reverse-bias voltages with a fixed output current of 50 μA.

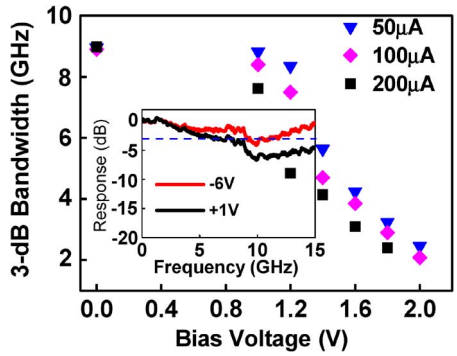

Fig. 6. Measured 3-dB O–E bandwidth versus forward-bias voltage for the linear cascaded device under different output photocurrents. The inset shows the measured O–E frequency responses of the linear cascaded device under forward- and reverse-bias voltages with a fixed output current of 50 μA.

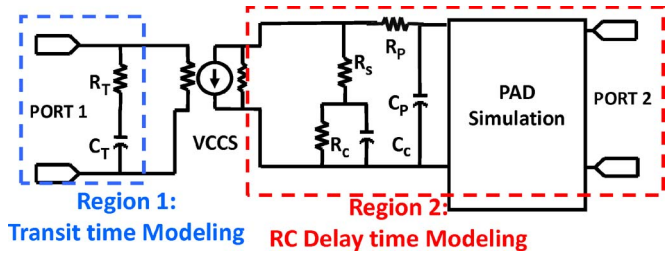

Fig. 7. Two-port small-signal equivalent-circuit model of our device, where VCCS indicates the voltage-controlled current source.

twice higher than that of a single cell with around one half of the responsivity. This is because the optical power needs to be about two times higher to feed each single cell in the cascaded structure to generate the same amount of output photocurrent as that of the single device. Fig. 4(a) and (b) shows the measured O–E power-conversion efficiency versus bias voltage of the single- and two-LPC cascaded devices under different optical pumping power values. As shown, the maximum O–E power-conversion efficiency of both devices under low pumping power and optimum bias voltage is around 34%. On the other hand, when the injected optical power exceeds 0.5 mW, as shown in Figs. 3 and 4, a significant reduction in both the photocurrent and external efficiency can be observed.

This phenomenon is somewhat similar to the case of our LPC, which has a smaller turn-on voltage, and can be attributed to the saturation of the device under high-optical-power injection. Under high-power injection, the space-charge field induced by the photogenerated carriers, which has the same direction as the external forward-bias voltage [17], should become stronger and aid the forward-bias operation of the device. We can thus observe that the forward-bias current, which screens the photocurrent and degrades the efficiency performance, increases more rapidly with the forward-bias voltage. Figs. 5 and 6 show the measured O–E bandwidths of 3 dB versus forward operating voltage of single and linear cascaded LPCs under different output photocurrents. The insets show the typical measured O–E frequency responses of the single- and two-LPC linear cascaded devices under the same effective forward voltage (i.e., +0.5 and +1 V, which is half of the turn-on voltage) and reverse-bias voltage (i.e., −3 and −6 V). During measurement of the cascaded LPCs, the ratio of injected optical power to the two devices is around 1:1.2. The photogenerated signal was picked up from the PD with smaller injected power. It is shown that there is a significant bandwidth degradation for both devices with an increase in the forward bias (0 to +2 V) and the output photocurrent (i.e., 50 μA to around 0.5 mA). In addition, the linear cascaded LPCs exhibits a faster speed performance than the single PD under the same effective bias voltage, as shown in the insets in Fig. 6.

Under a bias of +1 V and an output photocurrent of 50 μA of the linear cascaded LPC, which corresponds to the bias of +0.5 V for the single device, the measured bandwidths of 3 dB for the cascaded and single devices are around 9 and 6 GHz, respectively. Even when the output photocurrent of the linear cascaded device reaches 0.2 mA at an operating voltage of +1 V, a 7.6-GHz 3-dB bandwidth can still be sustain. This is a clear indication of the capability of our linear cascaded LPC for 10-Gb/s data transmission under a bias voltage of +1 V. The equivalent-circuit modeling technique is used to investigate the mechanism for the observed bandwidth degradation in both devices under near the turn-on forward bias and the bandwidth enhancement effect with the cascaded device. Fig. 7 shows the established two-port equivalent-circuit model. Regions 1 and 2 in this model represent the bandwidth limitation of the carrier transit time f_t and resistive–capacitive (RC) delay time f_{RC}, respectively [14], [16]. The artificial RC network [i.e., R_T, C_T, and $I(f)$] in port 1 of region 1 represents the carrier transit-time effect. The S_{21} parameter is equivalent to the net O–E frequency response [14], [16], and the S_{22} parameter of region 2 determines the RC-limited frequency response of the device.

TABLE I
LIST OF VALUES OF ELEMENTS USED IN THE FITTING PROCESS IN THE EQUIVALENT-CIRCUIT MODEL OF OUR DEVICE UNDER A LOW OUTPUT PHOTOCURRENT (0.05 mA)

Parameter	Physical Meaning	Fitted Values			
Device type	Single-device of 2-Cascaded device	Single		2-Cascaded	
Bias point	Applied forward bias voltage (V)	0.5	1.0	1.0	2.0
Rc	Resistance of Collector Layer (kΩ)	6.2	0.5	5.0	1.59
Cc	Capacitance of Collector Layer (fF)	97.76	133.3	94.3	130.1
Rs	Contact Resistance (Ω)	110.8			
Cp	Parasitic Capacitance (fF)	73			
Rp	Parasitic Resistance (Ω)	32.7			
Pad Simulation	The simulated S-parameters by using Momentum software	--			

TABLE II
LIST OF VALUES OF ELEMENTS USED IN THE FITTING PROCESS IN THE EQUIVALENT-CIRCUIT MODEL OF OUR DEVICE UNDER HIGH OUTPUT PHOTOCURRENT (0.2 mA)

Parameter	Physical Meaning	Fitted Values			
Device type	Single-device of 2-Cascaded device	Single		2-Cascaded	
Bias point	Applied forward bias voltage (V)	0.5	1.0	1.0	2.0
Rc	Resistance of Collector Layer (kΩ)	6.2	0.5	5.0	0.8
Cc	Capacitance of Collector Layer (fF)	30	61	97	142.2
Rs	Contact Resistance (Ω)	110.8			
Cp	Parasitic Capacitance (fF)	73			
Rp	Parasitic Resistance (Ω)	32.7			
Pad Simulation	The simulated S-parameters by using Momentum software	--			

By assuming an ideal voltage-controlled current source (VCCS) (without the influence from (R_T and C_T) in region 2), we can thus get the RC-limited frequency response for the device based on the measured S_{22} parameter, as will be discussed in the following. The physical meaning of each component in region 2 has been detailed in our previous work [16].

The parameters for the "pad simulation" block include the parasitic effects of the coplanar-waveguide (CPW) pad integrated with the device active area. The S parameters for this block can be calculated using momentum simulation software [16]. The values for each circuit element in region 2 used in the fitting process can be found in Tables I and II. These tables show the fitting parameters used under different forward-bias voltages and low (0.05 mA) and high (0.2 mA) output photocurrents, respectively. The contact resistance (R_s) values for each device are chosen based on the measured differential resistance. In addition, the junction capacitance (C_c) values are chosen according to their active areas. As shown for both devices, such values become larger with an increase in the forward-bias voltage due to the narrowing of the depletion width. The values of the parasitic capacitance C_p are determined by the overlay of bottom n-type contact layers and the topmost connected metals from the p-contact layer to the CPW pads. Figs. 8 and 9 show the measured/fitted S_{22} parameters (from near dc to 15 GHz) on the Smith chart under these two different output photocurrents (i.e., 0.05 and 0.2 mA) and two forward-bias voltages (i.e., 0.5 and 1 V for the single device and 1 and 2 V for the cascaded device) for the single and linear cascaded devices. A broadband network analyzer (Agilent N5250C) is used to measure the electrical S_{22} parameters of these devices.

As shown in Figs. 8 and 9, all simulation results agree well with the measured ones from 0.04 to 15 GHz based on the adopted parameters shown in Tables I and II. In addition, under a moderate forward-bias voltage (i.e., +1 V for the cascaded device and +0.5 V for the single device), all the measured S_{22} parameters are close, which implies that both devices have a similar RC-limited bandwidth. This is because we pick up the photogenerated RF signal from only one of the two LPC cascaded structures, as aforementioned, and the measurement results should be similar with a single LPC. On the other hand, when the forward bias reaches near the turn-on voltage (+2 V for the cascaded device and +1 V for the single device), as

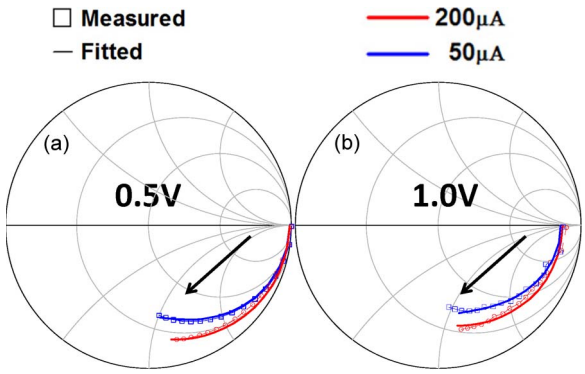

Fig. 8. Smith chart showing the measured (circles) and fitted (solid lines) S_{22} parameters for a single LPC under forward-bias voltages of (a) +0.5 and (b) +1 V. The output photocurrents in (a) and (b) are fixed at 0.2 and 0.05 mA. The direction of the arrowhead indicates the increase in sweeping frequency.

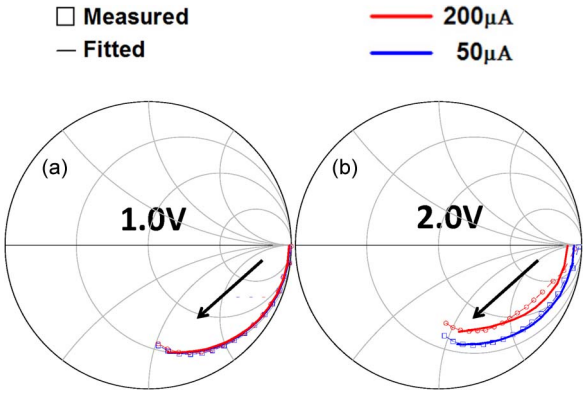

Fig. 9. Smith chart showing the measured (circles) and fitted (solid lines) S_{22} parameters for the linear cascaded device under forward-bias voltages of (a) +0.5 and (b) +1-V. The output photocurrents in (a) and (b) are both fixed at 0.2 and 0.05 mA. The direction of the arrowhead indicates the increase in sweeping frequency.

shown in Figs. 8(b) and 9(b), the measured S_{22} traces do not start from the open-circuit point on the Smith chart, due to the increase in forward conduction current. This leads to a reduction in the junction resistance R_c, as shown in Tables I and II. With the exception of the interesting bias-dependent behavior of the measured S_{22} parameters as aforementioned, the measured S_{22} parameter of the single device shows distinct power-dependent behaviors, as shown in Fig. 8. We can clearly see that, with the increase in the output photocurrent (0.05 to 0.2 mA), the S_{22} traces on the Smith chart are closer to those for the ideal open circuit than the measured S_{22} trace under low-current operation (0.05 mA), which implies a significant improvement in the microwave characteristics of the device.

As shown in Tables I and II, there is a significant reduction in the C_c values for the single device with the increase in its output photocurrent. This phenomenon seldom happens in the traditional p-i-n PD but has been reported in our previous work about near-ballistic unitraveling-carrier PDs (NBUTC PDs) [14]. In NBUTC PDs, the electrical field in the collector (depletion) layer is low enough to sustain an overshoot drift velocity even under a high reverse voltage (−3 V). A significant improvement in its RC-limited bandwidth with an increase in the output photocurrent has been observed, which can be attributed to the

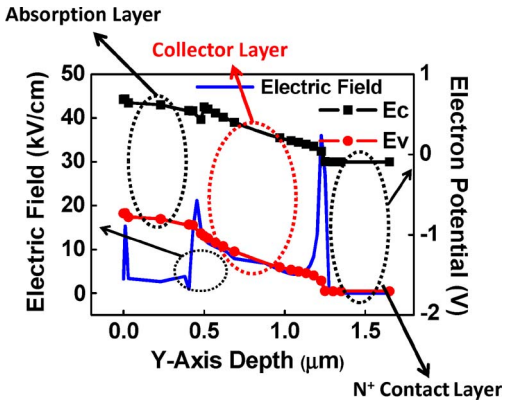

Fig. 10. Simulated band diagram of our single device under a forward bias of +0.8 V without injection light. The zero point on the Y-axis represents the interface between the air and the topmost p^+ ohmic contact layer.

ac capacitance reduction effect [14], [18]. It means the subtraction of the differential ac capacitance $I_C \times (d\tau_C/dV_{\rm ac})$ [14], [18], which is proportional to the current, from the junction capacitance C_c, where $V_{\rm ac}$ is the output ac voltage, I_C is the photocurrent, and τ_c is the electron drift time. In the case of the NBUTC PD, this effect should be significant due to the fact that under near-ballistic transport, the variation of the drift velocity (i.e., time is τ_c) of the electron versus the electrical field $V_{\rm ac}$ is obvious, according to the reported field-dependent electron drift velocity of III–V semiconductors. Fig. 10 shows the simulated band diagram and e-field distribution of our device under +0.8-V operation without the injection of optical power. This simulation is performed using a commercial computer-aided design (CAD) tool (ISE TCAD).[1] The simulated 1-D e-field and electron potential distributions shown here are located on the $x = 0$ axis of the device cross section, as shown in Fig. 2. As shown, the magnitude of the e-field in the $Al_{0.15}Ga_{0.85}As$-based collector layer is less than 10 kV/cm, which is close to the critical e-field for the overshoot drift velocity of electrons in the $Al_{0.15}Ga_{0.85}As$ layer [19]. We can thus expect that any high output ac photocurrent (voltage)-induced space-charge field should further screen the built-in e-field in the collector layer and greatly slow down the overshoot drift velocity of the electrons, which suggests that the ratio of electron drift time (velocity) to ac voltage $d\tau_C/dV_{\rm ac}$ should be large, and there would be a significant ac capacitance reduction. This phenomenon accompanies an improved RC-limited bandwidth in the single device; however, there is still a serious degradation in the net O–E bandwidth, as shown in Figs. 5 and 6. This is due to the fact that the dominant bandwidth-limiting factor is the internal carrier transient time rather than the RC time constant under forward bias, as will be discussed in the following.

On the other hand, for the cascaded devices, as shown in Fig. 9, this phenomenon is not significant. This result can be attributed to an imbalance in the optical power injected into the two cascaded devices (1:1.2), which causes the device with the lower injected optical power to suffer from a smaller effective dc or instantaneous ac forward voltage and a larger

[1]Synopsys, Inc., 700 East Middle field Rd., Mountain View, CA, 94043-4033, U.S.A.

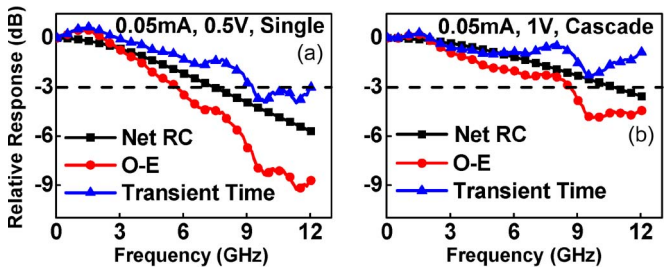

Fig. 11. Extracted RC-limited frequency responses, internal carrier transient-time responses, and measured O–E frequency responses for the (a) single and (b) cascaded devices under the same effective forward-bias voltage and (+0.5 V for the single device and +1 V for the cascade device) output photocurrent (0.05 mA).

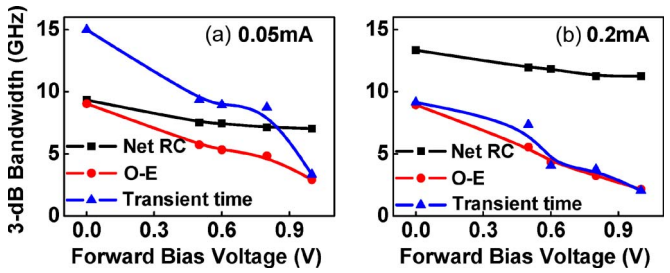

Fig. 12. Measured O–E bandwidth, extracted RC bandwidth, and transient-time-limited 3-dB bandwidth versus forward-bias voltages for the single device under (a) low (0.05 mA) and (b) high output photocurrents (0.2 mA).

built-in field compared with the device with a higher injected power. The larger built-in field should avoid the slowing down of the overshoot electron drift velocity and impede the ac capacitance reduction effect as aforementioned. We can thus understand that the cascaded structure exhibits a higher O–E bandwidth than that of the single device from zero bias to near forward conduction, as shown in Figs. 5 and 6, due to the faster internal carrier transient time. By using the extracted equivalent-circuit model in region 2, the RC-limited frequency responses, and the measured net O–E frequency responses, we can further determine the internal transient-time-limited frequency responses. Fig. 11(a) and (b) shows the extracted net RC-limited frequency responses, internal carrier transient-time frequency responses, and measured O–E responses of the single and cascaded devices under the same effective forward-bias voltage (+0.5 versus +1 V) and output photocurrent (0.05 mA). As shown, the faster speed performance of the cascaded device can be mainly attributed to the shorter internal carrier transient time, as aforementioned. Figs. 12 and 13 show the three aforementioned 3-dB bandwidths (i.e., O–E, RC, and transient time) versus forward-bias voltages of the single and cascaded devices under low and high output photocurrents, respectively. Overall, based on the measurement and modeling results, we can conclude that, when the output photocurrent of both devices reaches hundreds of microamperes (200 μA for our case), the dominant bandwidth-limiting factor becomes the internal carrier transient time. On the other hand, under a low output photocurrent (tens of microamperes), both the RC and internal transient time limit the measured O–E bandwidths. Furthermore, under a certain range of forward-bias voltages and output photocurrents, a significant ac capacitance reduction

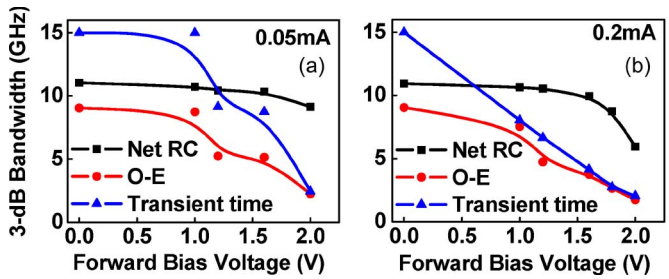

Fig. 13. Measured O–E bandwidth, extracted RC bandwidth, and transient-time-limited 3-dB bandwidth versus forward-bias voltages for the cascaded device under (a) low (0.05 mA) and (b) high output photocurrents (0.2 mA).

effect has been observed with the single device, which implies a significant reduction in the electron overshoot drift velocity and improvement in the RC-limited bandwidth. In addition, based on the extracted transient-time-limited bandwidths, as shown in Fig. 12, and the reported formulas for electron diffusion/drift time in the UTC PD [7], we can further determine the effective transient time in the active layer of our device. Take a single device under a low output photocurrent (0.05 mA) for example. The extracted transient-time-limited 3-dB bandwidth is around 10 GHz, which corresponds to an internal carrier transient time around of 55 ps. However, by using the equations for the electron drift/diffusion time given in [7], the minority electron diffusion coefficient (100 $\mathrm{cm^2V \cdot s}$) in p-type GaAs, electron thermal velocity (4.4×10^5 m/s), and electron drift velocity ($\sim 5 \times 10^4$ m/s) in the AlGaAs-based collector layer [20], we find that the calculated electron transient time is around 23 ps. Here, we used such a slow averaged electron drift velocity in the collector layer due to the fact that a low electric field in the collector layer and the happening of ac capacitance reduction, which implies a significant degradation in electron drift velocity, as discussed in Figs. 8 and 10. The discrepancy in the calculation and extracted carrier transient times (55 versus 23 ps) should be attributed to the carrier-trapping effect in the interface between collector layer and absorption layer, where there is a conduction band offset (discontinuity). This phenomenon will become more serious under forward-bias or high-power operation due to the reduction in the kinetic energy of the electrons and an increase in the effective barrier width (height) between such two layers [17].

One possible solution to minimize the carrier-trapping effect is to utilize the type-II band alignment in the absorption (base) and collector layers, which has already been demonstrated in the case of the UTC PD and heterojunction bipolar transistors [21], [22] with the capability of extremely high output current density and breakdown voltage [22]. Fig. 14(a) and (b) shows the measured bit error rate (BER) versus forward-bias voltage under different output photocurrents for the single device at 5 Gb/s and the linear cascaded device at 10 Gb/s (i.e., a pseudorandom bit sequence of $2^{15} - 1$). Figs. 15 and 16 show the corresponding error-free eye patterns at 5 and 10 Gb/s under different forward-bias voltages for the single and cascaded devices, respectively. During eye-pattern measurement, the devices were connected with low-noise (MITEQ: JSTD-30k1500-34-10P) and limiting amplifiers (Centellax: UXD20P) for good eye patterns. As shown in Fig. 15, the single device

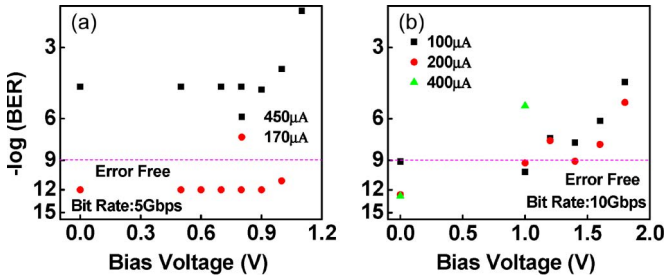

Fig. 14. Measured BER versus forward-bias voltages of (a) the single device at 5 Gb/s and (b) the linear cascaded device at 10 Gb/s under different output photocurrents.

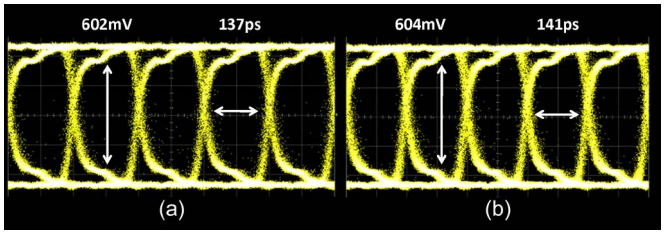

Fig. 15. Measured 5 Gb/s error-free eye patterns of the single device at (a) a bias of 0 V and (b) a forward bias of +1 V. The output photocurrent in both figures is fixed at 0.3 mA.

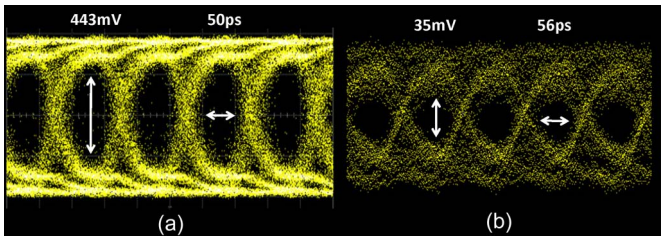

Fig. 16. Measured 10 Gb/s error-free eye patterns of the cascaded device at (a) a bias of 0 V and (b) a forward bias of +1 V. The output photocurrent in (a) and (b) is fixed at 0.4 and 0.1 mA, respectively.

can achieve a performance of 5 Gb/s error-free (BER $< 10^{-9}$) data transmission from the forward-bias voltage from 0 to +1 V with an output current of around 0.3 mA, which corresponds to a maximum O–E power-conversion efficiency of around 34%. On the other hand, using the linear cascaded structure, the error-free transmission data rate can be further boosted to 10 Gb/s under the same dc forward-bias voltage (+1 V). However, for 10-Gb/s operation, the required output photocurrent from our device must be as high as over 0.3 mA to drive the connected limiting amplifier (over its threshold voltage). Under zero-bias operation, 10-Gb/s error-free operation can be achieved with an output photocurrent of 0.4 mA and a clear 10-Gb/s eye opening is shown, as shown in Fig. 16(a).

On the other hand, when the bias voltage reaches +1 V and the output photocurrent reaches 0.4 mA, there is a serious speed degradation, which impedes the 10 Gb/s error-free eye opening. We thus remove the limiting amplifier and let the output photocurrent become as low as possible during the 10 Gb/s eye-pattern measurement to avoid the undesired bandwidth degradation. Fig. 16(b) shows the 10 Gb/s error-free eye pattern measured under a bias of +1 V and an output photocurrent of 0.1 mA without using the limiting amplifier.

IV. Conclusion

In conclusion, we have demonstrated a novel linear cascaded high-speed LPC, which can sustain high-speed and high-responsivity performance even under forward operation and generate dc electrical power. This result is better than the rule of high-speed PDs, which states that a device has to be operated under reverse bias, thus consuming power. Error-free data detection of 10 Gb/s and O–E power-generation efficiency of 21.1% can be achieved simultaneously at a forward bias of +1 V and an optical wavelength of 850 nm.

References

[1] C. L. Schow, F. E. Doany, C. Tsang, N. Ruiz, D. Kuchta, C. Patel, R. Horton, J. Knickerbocker, and J. Kash, "300-Gb/s, 24-channel full-duplex, 850-nm CMOS-based optical transceivers," in *Proc. OFC*, San Diego, CA, Feb. 2008, p. OMK5.

[2] M. Oda, J. Sakai, H. Takahashi, and H. Kouta, "Chip-to-chip optical interconnection for next-generation high-performance systems," in *Proc. Annu. Meeting IEEE LEOS*, Lake Buena Vista, FL, Oct. 2007, pp. 638–639.

[3] K. Kurata, "High-speed optical transceiver and systems for optical interconnects," in *Proc. OFC*, San Diego, CA, Mar. 2010, p. OThS3.

[4] H.-L. Hsiao, H.-C. Lan, C.-C. Chang, C.-Y. Lee, S.-P. Chen, C.-H. Hsu, S.-F. Chang, Y.-S. Lin, F.-M. Kuo, J.-W. Shi, and M.-L. Wu, "Compact and passive-alignment 4-channel × 2.5-Gbps optical interconnect modules based on silicon optical benches with 45° micro-reflectors," *Opt. Express*, vol. 17, pp. 24 250–24 260, Dec. 21, 2009.

[5] R. S. Tucker, "A green Internet," in *Proc. Annu. Meeting IEEE LEOS*, Newport Beach, CA, Nov. 2008, p. PLE3.

[6] J. A. Kash, A. F. Benner, F. E. Doany, D. M. Kuchta, B. G. Lee, P. K. Pepeljugoski, L. Schares, C. L. Schow, and M. Taubenblat, "Optical interconnects in exascale supercomputers," in *Proc. IEEE Photon. Soc. Meeting*, Denver, CO, Nov. 2010, pp. 483–484.

[7] H. Ito, S. Kodama, Y. Muramoto, T. Furuta, T. Nagatsuma, and T. Ishibashi, "High-speed and high-output InP-InGaAs unitraveling-carrier photodiodes," *IEEE J. Sel. Topics Quantum Electron.*, vol. 10, no. 4, pp. 709–727, Jul./Aug. 2004.

[8] F.-M. Kuo, T.-C. Hsu, and J.-W. Shi, "A GaAs/AlGaAs based uni-traveling-carrier photodiode for 10 Gbit/sec optical interconnect at 850 nm wavelength with zero electrical power consumption," in *Proc. OFC*, San Diego, CA, Mar. 2009, pp. 1–3.

[9] J.-W. Shi, F.-M. Kuo, T.-C. Hsu, Y.-J. Yang, A. Joel, M. Mattingley, and J.-I. Chyi, "The monolithic integration of GaAs/AlGaAs based uni-traveling-carrier photodiodes with Zn-diffusion vertical-cavity surface-emitting lasers with extremely high data-rate/power-consumption ratios," *IEEE Photon. Technol. Lett.*, vol. 21, no. 19, pp. 1444–1446, Oct. 2009.

[10] F.-M. Kuo, S.-S. Lo, C.-L. Pan, and J.-W. Shi, "Cascade laser power converter for simultaneous 10 Gbps data detection and efficient optical-to-electrical dc power generation," in *Proc. OFC*, Los Angeles, CA, Mar. 2010, p. JThA028.

[11] J. Schubert, E. Oliva, F. Dimroth, W. Guter, R. Loeckenhoff, and A. W. Bett, "High-voltage GaAs photovoltaic laser power converters," *IEEE Trans. Electron Device*, vol. 56, no. 2, pp. 170–175, Feb. 2009.

[12] D. Krut, R. Sudharsanan, W. Nishikawa, T. Isshiki, J. Ermer, and N. H. Karam, "Monolithic multi-cell GaAs laser power converter with very high current density," in *Proc. 29th IEEE Photovoltaic Spec. Conf.*, New Orleans, LA, May 2002, pp. 908–911.

[13] R. Sudharsanan, D. Krut, T. Isshiki, H. Cotal, S. Mesropian, A. Masalykin, and N. H. Karam, "A 53% high efficiency GaAs vertically integrated multi-junction laser power converter," in *Proc. Annu. Meeting IEEE LEOS*, Newport Beach, CA, Nov. 2008, p. MC3.

[14] Y.-S. Wu, J.-W. Shi, and P.-H. Chiu, "Analytical modeling of a high-performance near-ballistic uni-traveling-carrier photodiode at a 1.55 μm wavelength," *IEEE Photon. Technol. Lett.*, vol. 18, no. 8, pp. 938–940, Apr. 2006.

[15] J.-W. Shi, F.-M. Kuo, and M.-Z. Chou, "A linear cascade near-ballistic uni-traveling-carrier photodiodes with extremely high saturation-current bandwidth product (6825 mA-GHz, 75 mA/91 GHz) under a 50 Ω load," presented at the Optical Fiber Comunication, San Diego, CA, Mar. 2010, Paper PDPA6.

[16] F.-M. Kuo, M.-Z. Chou, and J.-W. Shi, "Linear-cascade near-ballistic uni-traveling-carrier photodiodes with an extremely high saturation-current-bandwidth product," *IEEE/OSA J. Lightwave Technol.*, vol. 29, no. 4, pp. 432–438, Feb. 2011.
[17] Y.-L. Huang and C.-K. Sun, "Nonlinear saturation behaviors of high-speed p-i-n photodetectors," *IEEE/OSA J. Lightwave Technol.*, vol. 18, no. 2, pp. 203–212, Feb. 2000.
[18] M. Achouche, V. Magnin, J. Harari, F. Lelarge, E. Derouin, C. Jany, D. Carpentier, F. Blache, and D. Decoster, "High performance evanescent edge coupled waveguide unitraveling-carrier photodiodes for $>$ 40-Gb/s optical receivers," *IEEE Photon. Technol. Lett.*, vol. 16, no. 2, pp. 584–586, Feb. 2004.
[19] S. Hava and M. Auslender, "Velocity-field relation in GaAlAs versus alloy composition," *J. Appl. Phys.*, vol. 73, no. 11, pp. 7431–7434, Jun. 1993.
[20] Y. A. Goldberg, *Handbook Series on Semiconductor Parameters*, M. Levinshtein, S. Rumyantsev, and M. Shur, Eds. London, U.K.: World Scientific, 1999, pp. 1–36.
[21] M. W. Dvorak, C. R. Bolognesi, O. J. Pitts, and S. P. Watkins, "300 GHz InP/GaAsSb/InP Double HBTs with High Current Capability and $BV_{CEO} \geq 6$ V," *IEEE Electron Device Lett.*, vol. 22, no. 8, pp. 361–363, Aug. 2001.
[22] L. Zheng, X. Zhang, Y. Zeng, S. R. Tatavarti, S. P. Watkins, C. R. Bolognesi, S. Demiguel, and J. C. Campbell, "Demonstration of high-speed staggered lineup GaAsSb-InP unitraveling carrier photodiodes," *IEEE Photon. Technol. Lett.*, vol. 17, no. 3, pp. 651–653, Mar. 2005.

Jin-Wei Shi was born in Kaohsiung, Taiwan, on January 22, 1976. He received the B.S. degree in electrical engineering and the Ph.D. degree from National Taiwan University, Taipei, Taiwan, in 1998 and 2002, respectively.

From 2000 to 2001, he was a Visiting Scholar with the University of California, Santa Barbara (UCSB), Santa Barbara. In 2002–2003, he was a Postdoctoral Researcher with the Electronic Research & Service Organization, Industrial Technology Research Institute. Since 2003, he was with the Department of Electrical Engineering, National Central University, Taoyuan, Taiwan, where he is currently an Associate Professor. In 2011, he joined the Department of Electrical and Computer Engineering, UCSB, again as a Visiting Scholar. He is the author or coauthor of more than 80 journal papers and 130 conference papers. He is a holder of 20 patents. His current research interests include ultrahigh-speed/power optoelectronic devices, such as photodetectors, electroabsorption modulators, submillimeter-wave photonic transmitters, and semiconductor lasers.

Dr. Shi was an Invited Speaker of the 2002 IEEE Laser and Electro-Optics Society, 2005 International Society of Optical Engineering (SPIE) Optics East, the 2007 Asia-Pacific Microwave Photonic Conference, and the 2008 Asia Optical Fiber Communication & Optoelectronic Exposition & Conference. He was a member of the Technical Program Committee of the Optical Fiber Conference from 2009 to 2011. He was a recipient of the 2007 Excellence Young Researcher Award from the IEEE Chinese Association and the 2010 Da-You Wu Memorial Award.

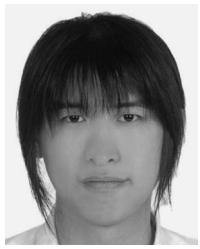

F.-M. Kuo was born in Kaohsiung, Taiwan, on February 12, 1986. He received the B.S. degree in electrical engineering from National Central University, Jhongli, Taiwan, where he is currently working toward the Ph.D. degree in electrical engineering.

His research interests include millimeter-wave high-power photodiodes (PDs) and their applications. He is also involved in radio-frequency/microwave semiconductor optoelectronic devices for communication, such as vertical-cavity surface-emitting lasers, avalanche PDs, and high-speed light-emitting diodes.

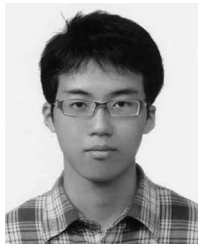

Chan-Shan Yang received the B.S and M.S. degrees both in engineering from the Institute of Electro-Optical Engineering, National Chiao Tung University, Hsinchu, Taiwan, in 2007 and 2008, respectively. He is currently working toward the Ph.D. degree with the Department of Physics, National Tsing Hua University, Hsinchu.

His research interests include ultrafast lasers and their applications in terahertz photonics, solar cells, optical communication, and physical properties of liquid crystals.

S.-S. Lo, photograph and biography not available at the time of publication.

Ci-Ling Pan (M'88–SM'03) received the Ph.D. degree in physics from Colorado State University, Fort Collins, in 1979.

In 1992–1995, he was the Director with the Institute of Electro-Optical Engineering (IEO), National Chiao Tung University (NCTU), Hsinchu, Taiwan. In 2004–2006, he was the founding Chair with the Department of Photonics, NCTU. He was also a University Chair Professor with the DOP and IEO, NCTU. Since February 2009, he has been with the Department of Physics, National Tsing Hua University (NTHU), Hsinchu. In particular, his group has recently developed numerous devices for laser and THz photonics with liquid crystal enabled functionalities. He has also taken sabbatical leaves with the University of California, Berkeley; Osaka University, Suita, Japan; and the Chinese University of Hong Kong, Shatin, Hong Kong. His research interests include lasers and their applications in broadband optical communication, precision metrology, and ultrafast and terahertz photonics.

Dr. Pan has been a member of the Phi Tau Phi Honor Society since 1991 and a Fellow of the Photonic Society of Chinese Americans since 1998, the Optical Society since 2004, the International Society of Optical Engineering since 2004, and the Physical Society of Republic of China since 2005. He was a recipient of the Merit Research Fellow Award of the National Science Council in 2002; the Academics Award of the Ministry of Education and the Engineering Medal by the Optical Engineering Society, Taiwan, in 2004; the Outstanding Engineering Professor Award of the Chinese Institute of Engineers in 2006; and the Pan Wen Yuan Foundation Research Excellence Award in 2007.